

# MatSwap: Light-aware material transfers in images

IVAN LOPES, Inria, France

VALENTIN DESCHAINTE, Adobe Research, UK

YANNICK HOLD-GEOFFROY, Adobe Research, Canada

RAOUL DE CHARETTE, Inria, France

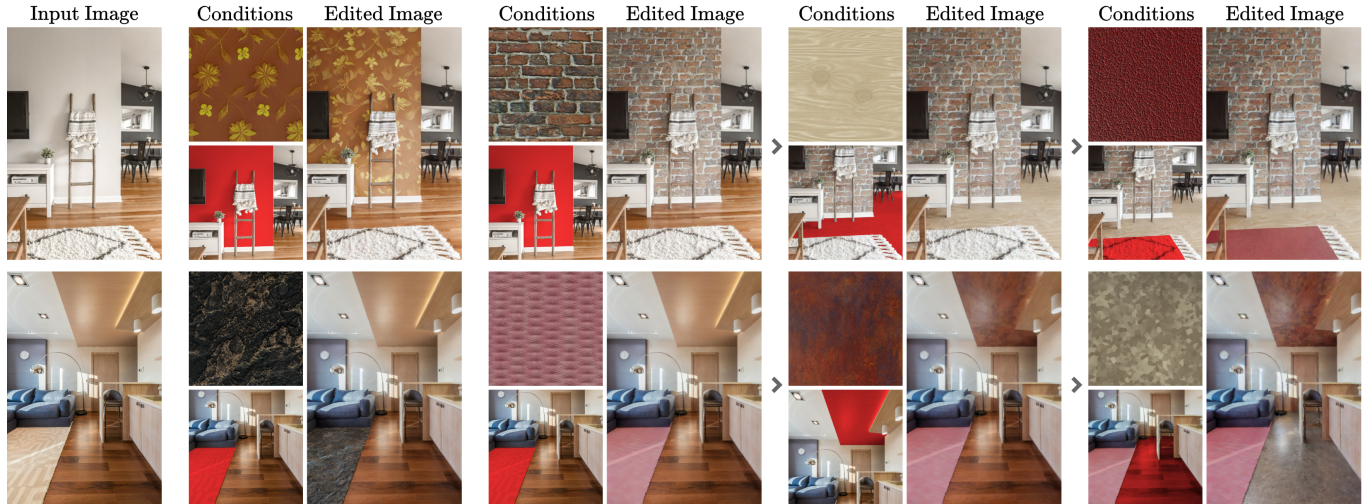


Fig. 1. MatSwap allows realistic material transfer in images. From an input image (left), our method seamlessly integrates an exemplar material (top left inset) into the user-specified region (red mask, bottom left inset). We can plausibly replace the wall’s surface (top) with tapestry (first result) or bricks (second), and also alter the wood type on the floor (third) and the mat (rightmost). Similarly, we present two distinct material swaps for the carpet (bottom row), and further modify our second result by changing the ceiling and floor (rightmost). MatSwap photorealistically handles lighting effects such as low-frequency shading (wall, top row) and cast lights (mat, bottom row).

We present MatSwap, a method to transfer materials to designated surfaces in an image photorealistically. Such a task is non-trivial due to the large entanglement of material appearance, geometry, and lighting in a photograph. In the literature, material editing methods typically rely on either cumbersome text engineering or extensive manual annotations requiring artist knowledge and 3D scene properties that are impractical to obtain. In contrast, we propose to directly learn the relationship between the input material—as observed on a flat surface—and its appearance within the scene, without the need for explicit UV mapping. To achieve this, we rely on a custom light- and geometry-aware diffusion model. We fine-tune a large-scale pre-trained text-to-image model for material transfer using our synthetic dataset, preserving its strong priors to ensure effective generalization to real images. As a result, our method seamlessly integrates a desired material into the target location in the photograph while retaining the identity of the scene. We evaluate our method on synthetic and real images and show that it compares favorably to recent work both qualitatively and quantitatively. We will release our code and data upon publication.

## 1 INTRODUCTION

Photographs capture the visual appearance of a scene by measuring the radiant energy resulting from the complex interaction of light, geometry, and materials. Among others, textures and materials are

key components that contribute to the aesthetics and emotions conveyed by images [Joshi et al. 2011]. Unfortunately, their appearances are largely entangled with the scene’s lighting and geometry, making it difficult to edit a posteriori.

Recently, the editing or generation of images has been significantly simplified by advancements in diffusion models that can benefit from internet-scale datasets [Schuhmann et al. 2022]. Such models can be used for prompt-guided diffusion inpainting, where only part of an image is modified to follow user guidance [Lugmayr et al. 2022; Meng et al. 2022]. However, textually describing a material is not trivial, especially when it exhibits complex patterns or appearance. An alternative is to use pixel-aligned maps to drive the generation. Using ControlNet [Zhang et al. 2023] such conditions can come in the form of semantics (*e.g.*, segmentation maps), visual maps (*e.g.*, edges), or geometry information (*e.g.*, depth, normal). IP-Adapter [Ye et al. 2023] proposes a similar approach for global conditioning, where CLIP [Radford et al. 2021] visual embeddings are used as an effective guidance signal for image generation. ZeST [Cheng et al. 2024] builds on the latter, showing that material inpainting can be conditioned with a CLIP encoder to extract a material appearance from an image. However, this offers little control to the artist over the transferred material appearance (*e.g.*, scale, rotation). To achieve greater control, RGB $\leftrightarrow$ X [Zeng et al. 2024] proposes to directly modify the estimated PBR maps, at the cost of

Authors’ addresses: Ivan Lopes, Inria, France, ivan.lopes@inria.fr; Valentin Deschainte, Adobe Research, UK, deschaint@adobe.com; Yannick Hold-Geoffroy, Adobe Research, Canada, holdgeof@adobe.com; Raoul de Charette, Inria, France, raoul.de-charette@inria.fr.

manual per-pixel editing. However, such an approach is impractical for spatially varying materials, as manual editing requires careful geometry and perspective texture projection handling.

In this work, we introduce MatSwap, an exemplar-based method that improves material transfer in images while simplifying its usage and offering more controllability to the user. Given an image and a texture sample rendered or photographed on a mostly flat surface, our method inpaints a region of the image using the texture sample (*c.f.* Fig. 1), ensuring a close alignment with the original geometric and illumination cues obtained from off-the-shelf single image estimators [He et al. 2025; Zeng et al. 2024].

More precisely, we rely on a light- and geometry-aware diffusion model fine-tuned for generating realistic inpainted images. We fine-tune a pre-trained diffusion model [Rombach et al. 2022], which already incorporates priors about object appearances in images, using a new synthetic dataset. Our goal is therefore to specialize our model to the material transfer task while retaining its original priors for better generalization to real photographs. To train our model, we generate a procedural 3D dataset named PBRand, which consists of primitive shapes randomly arranged and lit with captured environment maps, and render pairs of images with varying materials applied on a randomly selected object surface. Finally, we compare MatSwap to state-of-the-art inpainting [flu 2024; Avrahami et al. 2023; Podell et al. 2024; Rombach et al. 2022] and the latest material transfer method [Cheng et al. 2024] showing that it outperforms them qualitatively and quantitatively.

Our approach enables material replacement in images through the following contributions:

- A lighting- and geometry-aware diffusion model that performs material transfer in a single image;
- A two-stage training pipeline based on synthetic data that generalizes to real images;
- PBRand, a new synthetic procedural dataset that provides 250,000 paired renderings suitable for training material replacement methods.

## 2 RELATED WORKS

### 2.1 Image generation and editing

Neural image generation received significant attention over the past decade, starting with GANs [Goodfellow et al. 2020; Karras et al. 2020] and more recently diffusion models [flu 2024; Podell et al. 2024; Rombach et al. 2022; Sohl-Dickstein et al. 2015] or normalizing flows [Esser et al. 2024; Zhang and Chen 2021]. Lately, diffusion models have become the *de facto* image generation framework [Betker et al. 2023; Peebles and Xie 2023; Podell et al. 2024; Ramesh et al. 2022], producing high-quality results and benefiting from internet-scale datasets [Schuhmann et al. 2022].

Controlling these image generation models became an active research field, first using text [Ho and Salimans 2021; Meng et al. 2022], then using various image modalities [Zhang et al. 2023] or physically-based rendering (PBR) properties [Zeng et al. 2024]. An effective approach to conditioning diffusion models is to train or fine-tune them with the desired control as input. For instance, using an image [He et al. 2025; Ke et al. 2024; Liu et al. 2024], or other scene properties [Zeng et al. 2024]. An alternative is to inject the

conditioning maps into the pre-trained frozen diffusion model, either using a parallel network [Zhang et al. 2023], an adapter [Ye et al. 2023], or via low-rank adaptation of the text encoder [Lopes et al. 2024]. Another control is to directly manipulate the input image embedding to modify its semantic properties [Guerrero-Viu et al. 2024]. Finally, operations on attention maps [Epstein et al. 2023; Hertz et al. 2022; Parmar et al. 2023] are also commonly used to manipulate parts of images during the generation process.

These conditionings can be coupled with the task of inpainting, when part of an image is generated to be seamlessly integrated into the input image. Generative diffusion models can be used for inpainting by compositing, at every denoising step, the estimated latent of the inpainted region with the latent of the input image [Lugmayr et al. 2022]. However, this leads to visible artifacts along the mask boundaries [Cheng et al. 2024]. Text-driven local image editing was proposed by Avrahami et al. [2023], blending latents in the masked and unmasked areas during the denoising process.

In this work, we fine-tune an existing diffusion model [Rombach et al. 2022] to perform material replacement. We incorporate additional inputs through zero-weight addition [Zhang et al. 2023]. To avoid the complexities of UV mappings linked to pixel-aligned conditionings, we leverage the priors of the diffusion model regarding object appearance, paired with global conditioning as suggested by IP-adapter [Ye et al. 2023], to define the desired material appearance.

### 2.2 Environment-aware image editing

Changing the appearance of a surface within an image is trivial in a 3D editor, but proves very challenging in photographs due to the complex interactions conflating appearance, light, and geometry.

**Lighting** plays a crucial role in photorealism and is a clear sign of forgery when not correctly handled [Kee et al. 2013]. When editing images, one way to encode lighting is through radiance, either using a parametric [Gardner et al. 2019; Griffiths et al. 2022; Poirier-Ginter et al. 2024] or non-parametric light model [Gardner et al. 2017; Pandey et al. 2021]. However, radiance is challenging for deep learning models due to its high dynamic range and spherical nature, making it difficult to map to the image plane. Inspired by intrinsic image decomposition, recent image editing methods chose irradiance as encoded by shading maps to represent illumination and perform object insertion [Fortier-Chouinard et al. 2024; Zhang et al. 2025] or relighting [Kocsis et al. 2024; Ponglertnapakorn et al. 2023; Yu et al. 2020]. Our method uses this same irradiance representation, estimating shading maps using RGB $\leftrightarrow$ X [2024].

**Material** replacement is a long-standing problem in Computer Graphics [An and Pellacini 2008; Khan et al. 2006] with early methods proposing to adjust materials reflectance of color [An and Pellacini 2008] through user scribble and edit propagation, or changing materials to metallic or glossy [Khan et al. 2006]. Leveraging deep learning, methods were proposed to edit materials in photographs, often targeting textures [Guerrero-Viu et al. 2024] or objects [Cheng et al. 2024; Delanoy et al. 2022; Sharma et al. 2024]. On a scene scale, RGB $\leftrightarrow$ X [2024] proposed using PBR maps as control, enabling the per-pixel change of material properties, in particular the albedo. However, this requires manual editing, which is impractical for textures or perspective-distorted objects. Closest to our work is

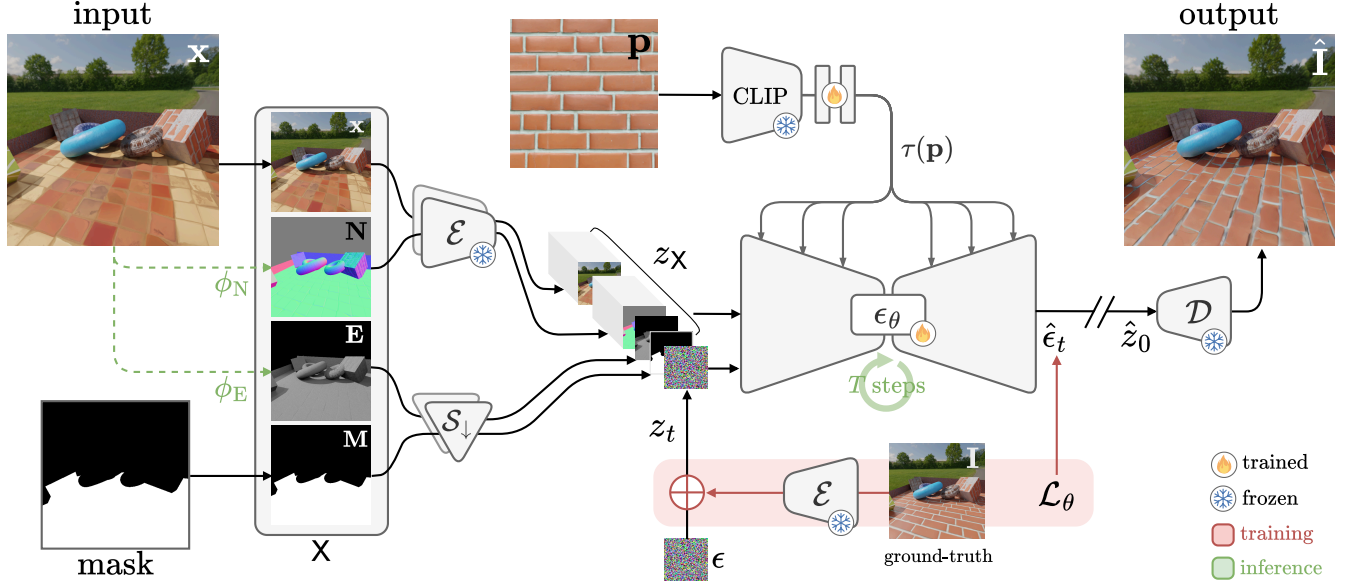


Fig. 2. Overview of MatSwap. We learn to transfer the material  $p$  on a given region  $M$  of an input image  $x$  by training a lighting- and geometry-aware diffusion model, leveraging irradiance  $E$  and normal  $N$  maps. Once encoded ( $\mathcal{E}$ ) or downsampled ( $S_{\downarrow}$ ), the image, mask, and maps are concatenated into a scene descriptor  $z_X$  which, together with the noise latent  $z_t$ , serve as input of the denoising UNet,  $\epsilon_{\theta}$ . To integrate the exemplar conditioning, we inject the visual CLIP features of the texture via adapter layers from IP-Adapter [Ye et al. 2023]. During inference, we leverage off-the-shelf estimators ( $\phi_N$ ,  $\phi_E$ ) to obtain normal and irradiance from real-world images.

ZeST [Cheng et al. 2024], which proposes a training-free method based on IP-Adapter to perform material transfer. It utilizes a depth-based ControlNet [Zhang et al. 2023], yet lacks explicit modeling of the scene illumination, leading to inaccurate shading and approximate material appearance. In contrast, our method uses off-the-shelf estimators to guide the diffusion with geometric and lighting cues, resulting in better transfers and fewer artifacts at the mask edges.

### 3 MATERIAL TRANSFER

Material transfer involves applying a material to a designated surface in an image, ensuring it integrates seamlessly into the scene. It can be seen as a form of 3D-aware inpainting, where a given material is plausibly blended within a target image while preserving its shading and geometry cues.

Specifically, given an exemplar texture image  $p$ , a target image  $x$ , and a target mask  $M$ , our material transfer consists of replacing the region defined by  $M$  in  $x$  with a material that resembles the exemplar texture image  $p$ . The mask is arbitrarily defined by the user and can cover either an object or a surface, or be obtained by an automatic segmentation method [Kirillov et al. 2023; Sharma et al. 2023]. None of the inputs require time-consuming annotations or expertise in 3D modeling, such as UV maps or texture wrapping.

To accomplish this, we build upon a latent diffusion model that encodes an image  $I$  into a latent space represented by an encoder:  $z_0 = \mathcal{E}(I)$ . From this point, we carry out iterative denoising as outlined in [Ho et al. 2020]. We start with a Gaussian-sampled latent vector  $z_T$  and aim to produce its denoised counterpart, the latent

vector  $z_0$ . This is a multi-step process, where a UNet predicts the residual  $\epsilon$  to denoise the latent variable at every step.

#### 3.1 MatSwap

We consider material transfer as a conditional generative task leveraging diffusion models. While the literature typically relies solely on geometrical cues [Cheng et al. 2024; Zhang et al. 2023] we observe that this can lead to inconsistent shading. Therefore, we guide our diffusion process with both scene illumination and geometry.

Assuming an image  $x$  of a scene, we describe it with a conditioning  $X$  which includes the target image and mask along with pixel-wise intrinsic maps representing normals  $N$  and diffuse irradiance  $E$ . Importantly, we ensure that these maps do not contain material information, avoiding to include properties such as albedo, roughness, or metalness. This ensures the diffusion is provided with enough information about the scene structure and illumination while remaining material-independent. Subsequently, as  $E$  we choose to represent only the diffuse illumination of the scene without specular effects since these are too correlated with materials, making it impractical to condition the model. We train our method on synthetic data (sec. 3.2), using the conditioning buffers readily provided by rendering engines while demonstrating that our model successfully generalizes to real images. For the latter, we leverage recent advances in single-image intrinsic channel estimation to obtain reasonably accurate maps from off-the-shelf methods such as  $RGB \leftrightarrow X$  [Zeng et al. 2024] or LoTUS [He et al. 2025]. Thus, for real images we define  $E = \phi_E(x)$  and  $N = \phi_N(x)$ , with  $\phi_N$  and  $\phi_E$  the normal and an irradiance estimators, respectively.

Next, we explain how to integrate the exemplar texture conditioning into the framework. Recently, IP-Adapter [Ye et al. 2023] demonstrated that image-prompt guidance could be accomplished by training adapters between the CLIP [Radford et al. 2021] visual encoder and the denoising UNet. Further works [Cheng et al. 2024; Guerrero-Viu et al. 2024; Vecchio et al. 2024; Yan et al. 2023] have shown that CLIP can be used to extract rich material features from images. Similarly, we condition our pipeline on the CLIP image embedding of the material we want to transfer in the target image. We replace the standard text cross-attention mechanism, injecting the visual CLIP features via adapter layers instead.

Our proposed method is illustrated in Fig. 2. We encode the ground-truth image  $I$  as  $z_0 = \mathcal{E}(I)$  and its scene descriptor stack  $X = \{\mathbf{x}, N, E, M\}$  describing our target image  $\mathbf{x}$ , defined as:

$$z_X = \left( \mathcal{E}(\mathbf{x}), \mathcal{E}(N), \mathcal{S}_\downarrow(E), \mathcal{S}_\downarrow(M) \right), \quad (1)$$

where  $\mathcal{E}$  is a pre-trained latent encoder and  $\mathcal{S}_\downarrow$  is a down-sampling operator. As seen in eq. (1) both the target image  $\mathbf{x}$  and normal maps  $N$  are encoded while the irradiance map  $E$  and the inpainting mask  $M$  are downsampled following previous works [Rombach et al. 2022; Zeng et al. 2024]. To provide the conditioning signal,  $z_X$  is concatenated to the noisy input latent  $z_t$  at every timestep  $t$ . The diffusion loss is defined as:

$$\mathcal{L}_\theta = \|\epsilon_t - \epsilon_\theta(z_t, z_X, t, \tau(\mathbf{p}))\|_2^2. \quad (2)$$

We write  $\epsilon_\theta$ , the denoising UNet, with its parameters  $\theta$ . It receives two kinds of inputs: the noisy image  $z_t$  concatenated with the scene descriptor  $z_X$ ; and a global conditioning via the cross-attention layers of  $\epsilon_\theta$  containing the timestep  $t$  and a CLIP embedding  $\tau(\mathbf{p})$ , with  $\mathbf{p}$  being the exemplar texture image. To condition the diffusion process with visual features, we initialize the adapter weights with those from IP-Adapter [Ye et al. 2023] and freeze the image encoder. In our pipeline, we train the full UNet and drop the text prompt to rely exclusively on the image prompt embedding  $\tau(\mathbf{p})$ , for which we train adapter layers, as seen Fig. 2 *top*.

Our end-to-end training method uses modality dropout on the input latents of  $z_X$  [Zeng et al. 2024] by randomly setting these to null vectors. This ensures the model can inpaint the target region with partial conditioning or even completely unconditionally.

### 3.2 Dataset

To train our method, we need paired images showing the same scene with identical lighting but with a known material change. We design a simple procedural 3D dataset in Blender, named PBRand, consisting of 250,000 scene pairs which we render along with irradiance, normals, UV and material segmentation maps. Scenes are created by randomly placing 3D primitives and lights within the boundaries of a cubic scene, and randomly varying the wall heights to allow direct lighting and occlusions. The images are rendered with image-based lighting [Debevec 2008] using a randomly rotated environment map sampled from a set of 100 HDRIs [pol 2025]. We use approximately 4,000 unique materials from MatSynth [Vecchio and Deschaintre 2024], randomly assigned to all objects. For each scene, one of the objects is randomly selected, and its material is replaced with another. This generates two buffers per scene, each

containing  $(\mathbf{x}, N, E, M, \mathbf{p}, I)$  with only the material on the selected object changed. We show samples from our dataset in Fig. 3.

To enforce consistency between the scale of the conditioning image and the rendered texture, we measure the texture coverage from the scene UV buffer and scale the exemplar image  $\mathbf{p}$  accordingly, similarly to recent work [Ma et al. 2024]. This ensures that the rendered texture appears at the same scale as in the conditioning image (e.g., a brick texture will have roughly the same number of tiles in  $\mathbf{p}$  and  $I$ ). Despite the simplicity of PBRand, we found it sufficient for our model to learn strong priors for material transfer.

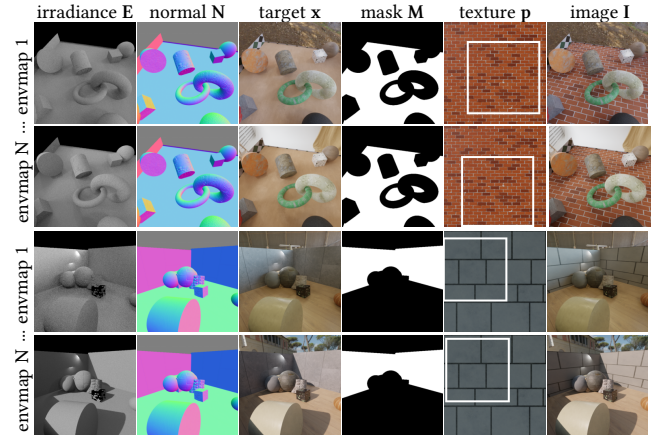


Fig. 3. Procedural dataset. We show examples of our PBRand dataset, which we use for training. It consists of primitive objects (spheres, cubes, cylinders, and tori) with random placements, orientations, and materials enclosed within four walls of varying heights. A total of 50,000 3D scenes were created in Blender, each rendered under 5 light variations, with image-based lighting to achieve realistic occlusions and cast shadows. For every scene, we render a second scene identical to the first, except for one object for which we swap the material. Under “texture  $\mathbf{p}$ ”, we show the full texture as well as a crop (outlined in white) that has a matching scale with the rendered surface.

### 3.3 Implementation Details

Our approach is based on Stable Diffusion [Rombach et al. 2022], a large publicly available text-to-image model. Specifically, we fine-tune from the IP-Adapter [Ye et al. 2023] checkpoint. Drawing inspiration from ControlNet [Zhang et al. 2023], we initialize additional convolutions with zero-convs. We train in two phases: first at a resolution of  $256 \times 256$  px for 100k iterations, followed by 50k iterations at  $512 \times 512$  px resolution. The training employs a batch size of 64 and spans roughly five days on an Nvidia A100 GPU accelerator. The AdamW optimizer [Kingma 2015; Loshchilov et al. 2019] is used with a learning rate of  $2 \times 10^{-5}$ .

To enhance robustness, we apply horizontal flipping as data augmentation, taking care to adjust the normals accordingly. Additionally, we implement a 10% probability of dropping all the conditioning inputs except the mask, along with another 10% chance of dropping any of the inputs:  $E, N, \mathbf{x}, \mathbf{p}$ . To drop  $\mathbf{p}$ , we set the CLIP embedding to the null vector. The mask  $M$  is always retained as input.

Our input  $\mathbf{p}$  corresponds to a material rendered on a flat surface covering the whole image in a fronto-parallel setting, illuminated

| Method        | Synthetic       |                    | Real              |
|---------------|-----------------|--------------------|-------------------|
|               | PSNR $\uparrow$ | LPIPS $\downarrow$ | CLIP-I $\uparrow$ |
| SD v2.1       | 18.16           | 0.2214             | 0.7611            |
| SD-XL inpaint | 19.10           | 0.2025             | 0.7462            |
| FLUX.1 Fill   | <u>19.92</u>    | <u>0.1825</u>      | 0.7552            |
| Blended LD    | 19.57           | 0.2282             | 0.7303            |
| ZeST          | 19.10           | 0.1879             | <u>0.7790</u>     |
| <b>ours</b>   | <b>20.62</b>    | <b>0.1783</b>      | <b>0.7994</b>     |

Table 1. Inpainting results. Comparison to baselines on inpainting capability of the proposed approach on synthetic and real scenes for material transfer.

| Method        | PSNR $\uparrow$ | LPIPS $\downarrow$ |
|---------------|-----------------|--------------------|
| SD v2.1       | 16.79           | 0.1275             |
| SD-XL inpaint | 18.86           | 0.1010             |
| FLUX.1 Fill   | <u>20.93</u>    | <u>0.0821</u>      |
| Blended LD    | 20.40           | 0.0847             |
| ZeST          | 18.84           | 0.0962             |
| ours w/o E    | 18.94           | 0.0925             |
| <b>ours</b>   | <b>21.43</b>    | <b>0.0668</b>      |

Table 2. Reliability to image irradiance. We estimate a model result’s irradiance map, *i.e.*,  $\phi_E(\hat{\mathbf{I}})$ , and measure its difference compared to the irradiance of the original image, *i.e.*,  $\phi_E(x)$ . This evaluates the adherence of the model to the illumination existing in the scene.

with a random HDRI from PolyHaven [pol 2025]. During training, we utilize the materials from MatSynth [Vecchio and Deschaintre 2024], from which we extract 16 random crops. To account for the scene scale in the reference image  $x$ , we extract the UV coordinates of each material within the image, and resize all material samples  $p$  by a factor of  $(\max(\text{UV}) - \min(\text{UV}))^{-1}$  in both horizontal and vertical dimensions. These exemplars are then resized to 224×224 px for input into CLIP.

## 4 EXPERIMENTS

We now compare our method against state-of-the-art inpainting and material transfer methods.

**Baselines.** For inpainting models, we consider version 2.1 of Stable Diffusion [Rombach et al. 2022], the official inpainting fine-tuning of SD-XL [Podell et al. 2024], the inpainting FLUX.1 model from Black Forest Labs [flu 2024], and Blended Latent Diffusion [Avrahami et al. 2023]. We also compare against ZeST [Cheng et al. 2024], the current state-of-the-art on material transfer. We employ the original models provided by the authors in all cases.

**Data.** We conduct our quantitative analysis on 300 pairs of synthetic renders and 50 real images. The synthetic test set includes artist-made 3D scenes [eve 2024] rendered with Blender’s physically-based Cycles renderer [2024]. We render the images and the ground truth normals and irradiance maps. Unless stated otherwise, the real images are sourced from the Materialistic evaluation set [Sharma et al. 2023]. All our evaluation data will be publicly released.

|                   | Train |      | Maps |   |   | Metrics         |                    |
|-------------------|-------|------|------|---|---|-----------------|--------------------|
|                   | IP-A  | UNet | M    | N | E | PSNR $\uparrow$ | LPIPS $\downarrow$ |
| (A <sub>1</sub> ) | ✓     |      |      |   |   | 19.06           | 0.3560             |
| (A <sub>2</sub> ) |       | ✓    |      |   |   | 18.81           | 0.3626             |
| (A <sub>3</sub> ) | ✓     | ✓    |      |   |   | 18.70           | 0.3642             |
| (A <sub>4</sub> ) | ✓     | ✓    | ✓    |   |   | 20.04           | 0.3277             |
| (A <sub>5</sub> ) | ✓     | ✓    | ✓    | ✓ |   | 19.91           | 0.3284             |
| (A <sub>6</sub> ) | ✓     | ✓    | ✓    |   | ✓ | <u>20.28</u>    | 0.3281             |
| (A <sub>7</sub> ) |       | ✓    | ✓    | ✓ | ✓ | 20.22           | <b>0.3243</b>      |
| (A <sub>8</sub> ) | ✓     | ✓    | ✓    | ✓ | ✓ | <b>20.38</b>    | <u>0.3256</u>      |

Table 3. Ablation study. We evaluate our main architectural and design decisions. All ablations are trained on the full set for 50k iterations. Our approach significantly benefits from the addition of the irradiance information (A<sub>6</sub>). The use of a mask as input rather than using a masked loss (A<sub>1,2,3</sub>) also significantly improves our material transfer quality (A<sub>4</sub>).

**Metrics.** We evaluate synthetic data using PSNR and LPIPS. Given that real data lacks ground truth maps, we evaluate its appearance using CLIP-I [Radford et al. 2021] by computing the cosine similarity score between the exemplar image and a crop of the generated region. Additionally, we compare its estimated irradiance to that of the original target image to assess the adherence to lighting cues.

Quantitative results are reported in Tab. 1. For this experiment, all conditionings are supplied to the methods. While inpainting methods provide competitive performance, they do not perform as well as specialized methods for material transfer. On synthetic data, FLUX.1 shows competitive performance, beating even ZeST, which specializes in material transfer. On this data, our method achieves a +3.5% and +2.4% improvement in PSNR and LPIPS, respectively. On real data, we offer an improvement of +2.6% on the CLIP-I measure over ZeST, the second best-performing method. Our method establishes a new state-of-the-art on all metrics evaluated.

We further evaluate the shading error produced by each method in Tab. 2. This error is determined by comparing the estimated irradiance maps of the output image  $\phi_E(\hat{\mathbf{I}})$  and the reference image  $\phi_E(\mathbf{I})$ . We observe that newer inpainting methods based on FLUX.1 and Blended LD preserve the illumination from the original image well. Our method, guided by the irradiance map E, understandably outperforms all compared methods in illumination preservation.

We present qualitative results in Fig. 9. We note that earlier inpainting methods such as Stable Diffusion based methods (SD v2.1, SD-XL inpaint) have trouble with perspective projection, often offering an orthographic view of the material pasted directly into the region (second, third, and sixth rows), greatly hindering the realism of the edits. Newer methods such as FLUX.1 and Blended LD better adhere to the scene’s geometry, but either lack perspective for FLUX.1 (sixth row) or differ from the exemplar material  $p$  (third to seventh rows). ZeST generally provides good geometry coherence, but exhibits artifacts (second, fourth, and seventh rows). In addition to good perspective projection (sixth row) and good respect for the exemplar material  $p$  (fourth row), our method MatSwap provides more complex lighting interactions as reflections and highlights

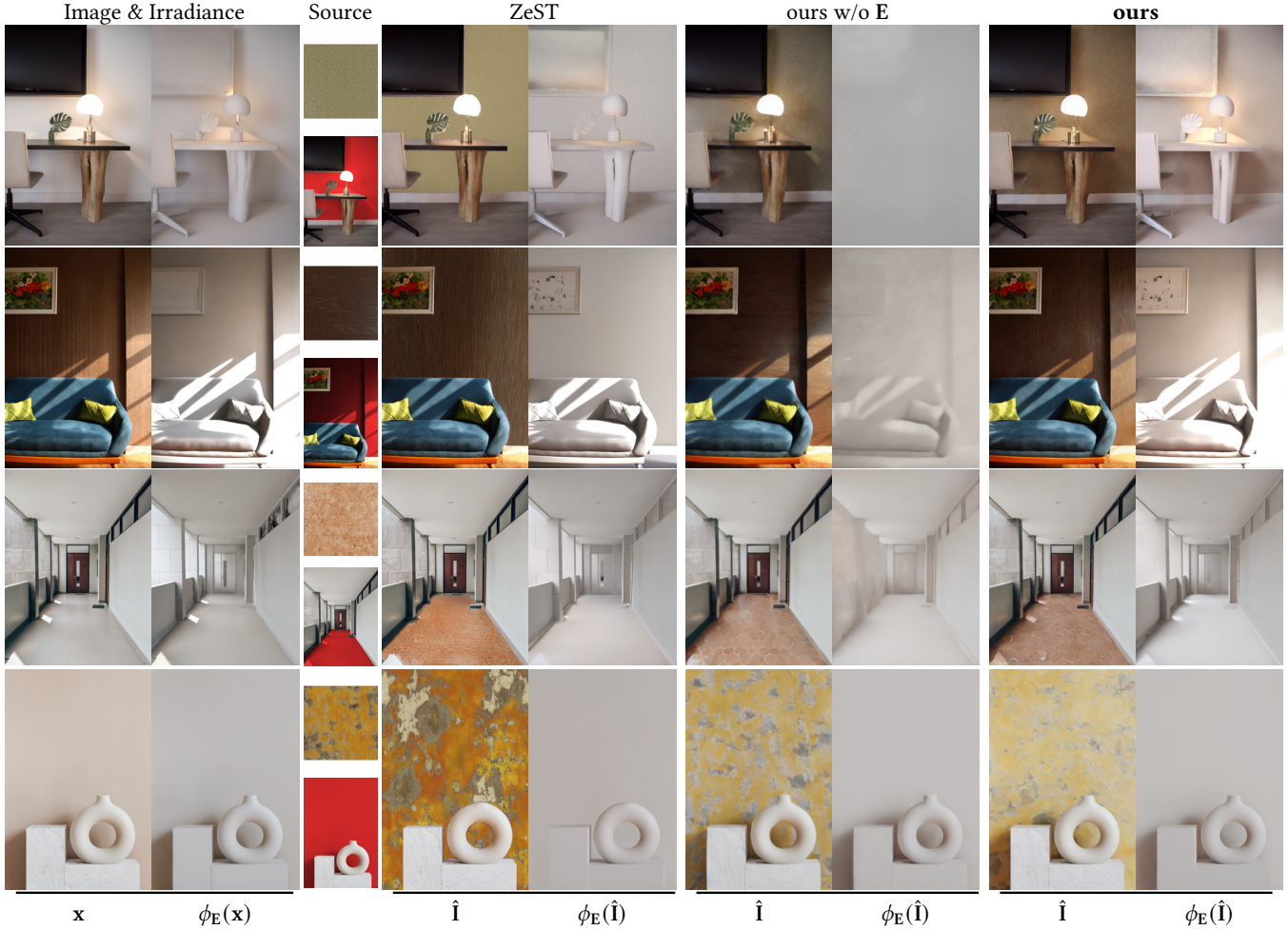


Fig. 4. Reliance on irradiance. We compare the irradiance of the input image  $x$  directly against the irradiance estimated from the images  $\hat{I}$  edited by ZeST and our model, both with or without irradiance  $E$ . Our approach better preserves the illumination of the input image, thanks to the irradiance information.

from lights (first and third rows). In general, MatSwap produces material transfers that blend well with their surroundings while preserving illumination on the applied material.

Additional analysis on color control can be found in Fig. 10. For these results, we convert the exemplar material  $p$  from RGB to HSV and change its hue. Our method respects the user-defined color well, seamlessly integrating it into the scene.

We evaluate the importance of the irradiance map  $E$  in Fig. 4. Our approach generates better matching shading than previous work, even without the irradiance map. However, high-frequency lighting effects from the original image such as highlights (first to third rows) require the irradiance map to be preserved.

Finally, we demonstrate our ability to control the scale of the inpainted material by adjusting the scale of the exemplar  $p$ . We evaluate this effect in Fig. 6 with three zoom levels. As our method processes larger features, it scales them up in the scene accordingly.

#### 4.1 Ablation study

We quantitatively evaluate the impact of each component of our method in Tab. 3. All ablations are trained on the entirety of our PBRand dataset, and evaluated on synthetic scenes. Unfreezing the UNet ( $A_2$ ) gives freedom for the image and mask to be used as conditionings ( $A_{4+}$ ), which significantly boosts performance. Further introducing the irradiance map  $E$  ( $A_6$ ) helps preserve the image shading, thus improving the results. Adding normals  $N$  ( $A_5$ ) improves the results slightly; we hypothesize its role is to disambiguate possible confusion between the geometry and the lighting. Overall, training the IP-Adapter encoders slightly improves the result compared to solely fine-tuning the denoising U-Net, keeping the IP-Adapter layers frozen with pretrained weights.

We explore the role of lighting conditioning in Fig. 5, showing that our model considers cues from both the target  $x$  and the irradiance map  $E$ . As expected, removing all lighting cues significantly deteriorates shading quality. We do so by masking the target region  $M$  in the target image  $x$  and removing the irradiance map  $E$ , that is using  $X = \{x \cdot M, N, M\}$ . The best results are obtained when

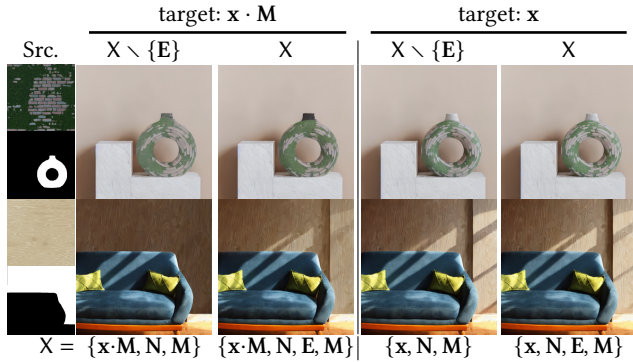


Fig. 5. Ablation study on lighting cues. When deprived of lighting cues by masking out the target image  $x$  (i.e., providing  $x \cdot M$  as target) and removing the irradiance map  $E$ , our method produces results with flat, implausible shading (leftmost). Reintroducing either the irradiance  $E$  (second column) or the masked region (third column) restores the light effects. Providing all lighting cues (MatSwap) provides the best result (rightmost). For clarity, we report the conditioning used below.

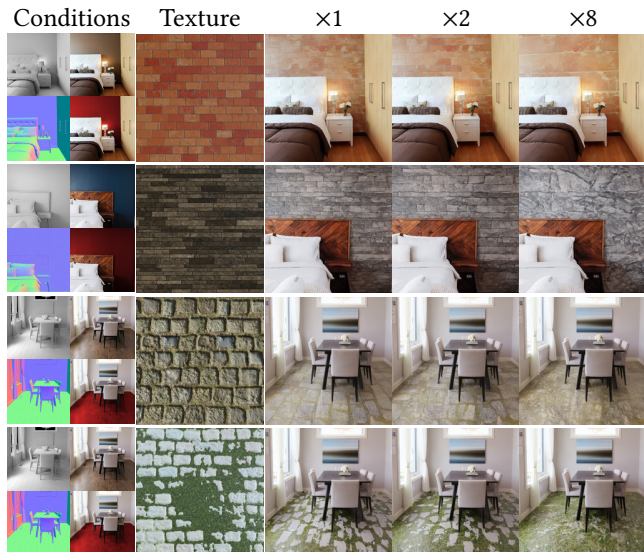


Fig. 6. Impact of exemplar  $p$  scale. We can implicitly control the 2D material appearance in the 3D scene by providing various the exemplar material  $p$  at different scales. We show results using the entire material ( $\times 1$ ), half the original material size ( $\times 2$ ), and one-eighth ( $\times 8$ ) and see that the transferred material scale follows that of the input.

both the full target image  $x$  (providing local geometry cues) and the irradiance (providing lighting information) are supplied.

## 5 LIMITATIONS

Despite exhibiting state-of-the-art performance in material transfer, our method still suffers from a few limitations that we illustrate in Fig. 8. A challenging case for us is surfaces pointing downwards or exhibiting high-frequency normals, both of which do not appear in our dataset and could benefit from a more extensive training set.



Fig. 7. Samples of our synthetic evaluation dataset scenes showing their diversity in appearance and illumination.

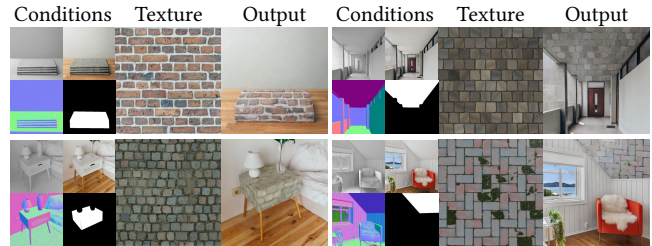


Fig. 8. Limitations. We illustrate our method’s limitations with objects with detailed normals being lost during material transfer (left column), and downward facing normals (right column). We believe these limitations could be mitigated by explicitly creating these situations in the training dataset.

Another challenge comes from thin or small objects that are difficult to process due to the diffusion model resolution and the downsizing of the input mask when working in latent space, effectively eroding the masked area. Finally, as we rely on normals and irradiance as inputs, our method is negatively impacted when they are poorly estimated. However, this is mitigated by the rapid progress in intrinsic image decomposition from which we directly benefit.

## 6 CONCLUSION

We present MatSwap, a method for material transfer from flat textures to images without requiring complex 3D understanding or UV mapping. Our approach naturally harmonizes the transferred material with the target image illumination, leveraging the available irradiance information. We demonstrate material transfer in real photographs with control over the scale and hue, making it easier to adapt the new material to the target scene. We believe our approach provides a more practical tool for artists to edit images and explore possible material variations, for example in the context of architecture visualization and interior design.

**Acknowledgments.** This research was funded by the French Agence Nationale de la Recherche (ANR) with the project SIGHT (ANR-20-CE23-0016) and performed with HPC resources from GENCI-IDRIS (Grants AD011014389R1 and AD011012808R3).

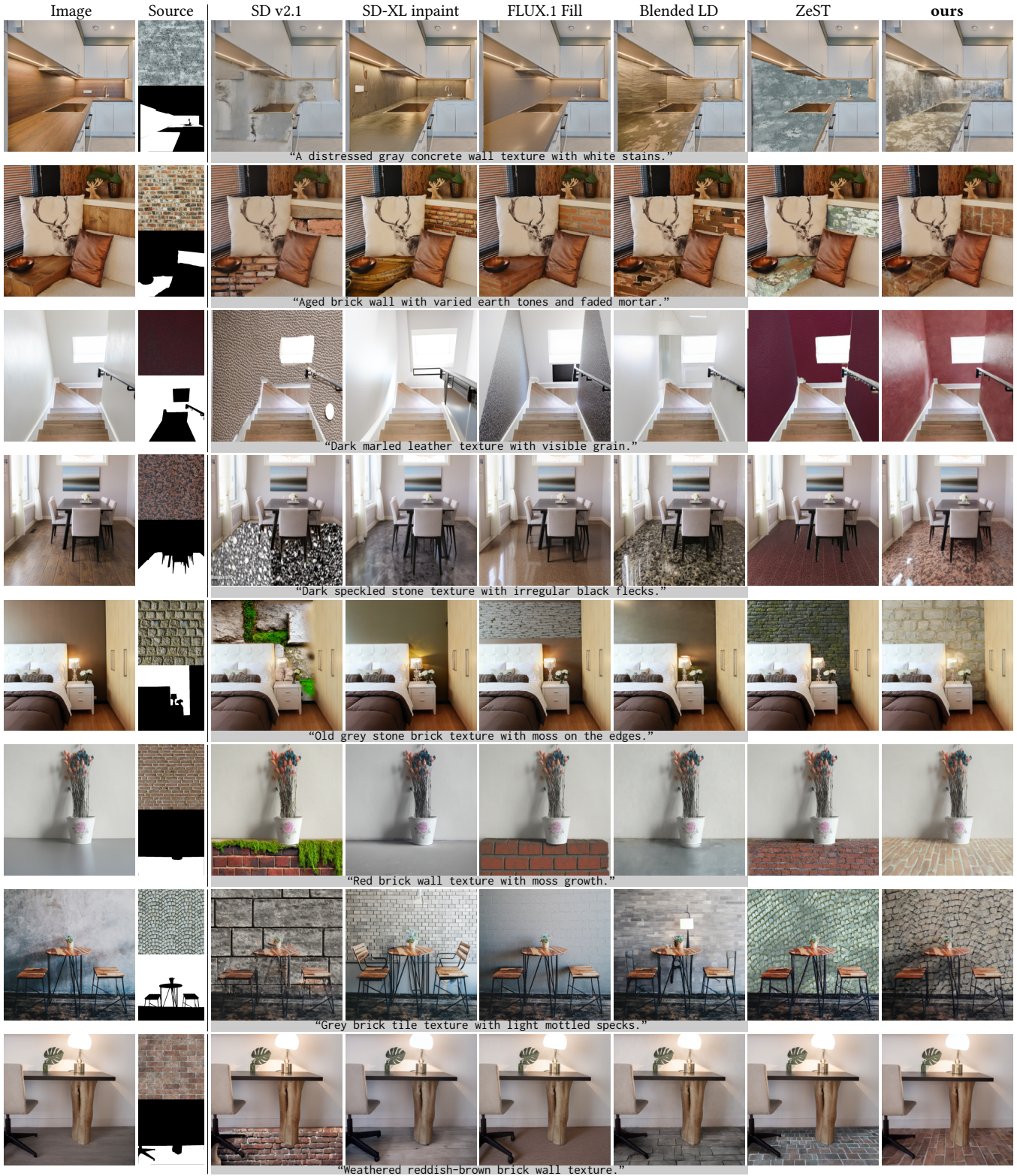


Fig. 9. Comparison to baselines. All methods use the input image and mask as conditioning: SD-v2.1, SD-XL, and ZeST use it to compose the final image at the latent space, while SD-XL, FLUX and ours use it as input. ZeST uses a depth map via its parallel ControlNet branch. Instead, we rely on both irradiance and normal maps at the input level of the UNet. We can see that text-based methods cannot precisely reproduce the desired appearance, as text descriptions tend to be too vague. Our approach better preserves the target image lighting while maintaining the transferred material appearance.



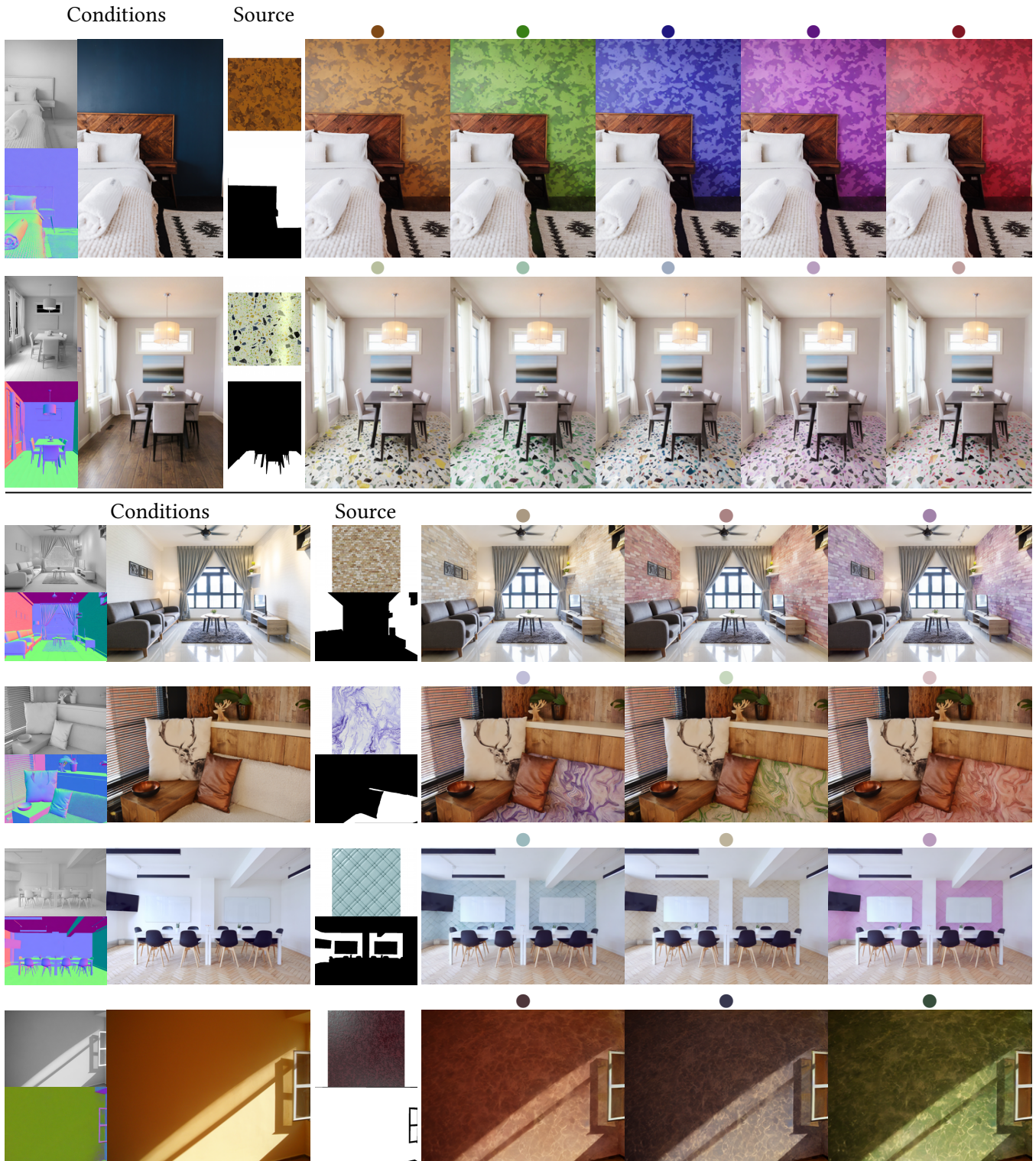


Fig. 10. Adherence to texture conditioning. We provide different hue variations of the exemplar material as input and observe that our method correctly adapts, maintaining realism in the generated image.

## REFERENCES

2024. Evermotion. <https://evermotion.org/>.
2024. FLUX.1. <https://huggingface.co/black-forest-labs/FLUX.1-dev>.
2025. Poly Haven. <https://polyhaven.com/>.
- Xiaobo An and Fabio Pellacini. 2008. Approp: all-pairs appearance-space edit propagation. In *SIGGRAPH*.
- Omri Avrahami, Ohad Fried, and Dani Lischinski. 2023. Blended latent diffusion. *ACM TOG* (2023).
- James Betker, Gabriel Goh, Li Jing, Tim Brooks, Jianfeng Wang, Linjie Li, Long Ouyang, Juntang Zhuang, Joyce Lee, Yufei Guo, et al. 2023. Improving image generation with better captions. *Computer Science* (2023).
- Blender. 1994-2024. *Blender - a 3D modelling and rendering package*. Blender Foundation. <http://www.blender.org>
- Ta-Ying Cheng, Prafull Sharma, Andrew Markham, Niki Trigoni, and Varun Jampani. 2024. Zest: Zero-shot material transfer from a single image. In *ECCV*.
- Paul Debevec. 2008. Rendering synthetic objects into real scenes: Bridging traditional and image-based graphics with global illumination and high dynamic range photography. In *SIGGRAPH*.
- Johanna Delanoy, Manuel Lagunas, Jorge Condor, Diego Gutierrez, and Belen Masia. 2022. A Generative Framework for Image-based Editing of Material Appearance using Perceptual Attributes. In *Computer Graphics Forum*.
- Dave Epstein, Allan Jabri, Ben Poole, Alexei Efros, and Aleksander Holynski. 2023. Diffusion self-guidance for controllable image generation. In *NeurIPS*.
- Patrick Esser, Sumith Kulal, Andreas Blattmann, Rahim Entezari, Jonas Müller, Harry Saini, Yam Levi, Dominik Lorenz, Axel Sauer, Frederic Boesel, Dustin Podell, Tim Dockhorn, Zion English, Kyle Lacey, Alex Goodwin, Yannik Marek, and Robin Rombach. 2024. Scaling Rectified Flow Transformers for High-Resolution Image Synthesis. In *ICML*.
- Frédéric Fortier-Chouinard, Zitian Zhang, Louis-Etienne Messier, Mathieu Garon, Anand Bhattad, and Jean-François Lalonde. 2024. SpotLight: Shadow-Guided Object Relighting via Diffusion. arXiv:2411.18665
- Marc-André Gardner, Yannick Hold-Geoffroy, Kalyan Sunkavalli, Christian Gagné, and Jean-François Lalonde. 2019. Deep parametric indoor lighting estimation. In *ICCV*.
- Marc-André Gardner, Kalyan Sunkavalli, Ersin Yumer, Xiaohui Shen, Emiliano Gamberetto, Christian Gagné, and Jean-François Lalonde. 2017. Learning to predict indoor illumination from a single image. *ACM TOG* (2017).
- Ian Goodfellow, Jean Pouget-Abadie, Mehdi Mirza, Bing Xu, David Warde-Farley, Sherjil Ozair, Aaron Courville, and Yoshua Bengio. 2020. Generative adversarial networks. *Commun. ACM* (2020).
- David Griffiths, Tobias Ritschel, and Julien Philip. 2022. OutCast: Outdoor Single-image Relighting with Cast Shadows. In *Computer Graphics Forum*.
- Julia Guerrero-Viu, Milos Hasan, Arthur Roullier, Midhun Harikumar, Yiwei Hu, Paul Guerrero, Diego Gutierrez, Belen Masia, and Valentin Deschaintre. 2024. Texsliders: Diffusion-based texture editing in clip space. In *SIGGRAPH*.
- Jing He, Haodong Li, Wei Yin, Yixun Liang, Leheng Li, Kaiqiang Zhou, Hongbo Liu, Bingbing Liu, and Ying-Cong Chen. 2025. Lotus: Diffusion-based Visual Foundation Model for High-quality Dense Prediction. (2025).
- Amir Hertz, Ron Mokady, Jay Tenenbaum, Kfir Aberman, Yael Pritch, and Daniel Cohen-Or. 2022. Prompt-to-prompt image editing with cross attention control. arXiv:2208.01626
- Jonathan Ho, Ajay Jain, and Pieter Abbeel. 2020. Denoising diffusion probabilistic models. *NeurIPS* (2020).
- Jonathan Ho and Tim Salimans. 2021. Classifier-Free Diffusion Guidance. In *NeurIPS Workshop*.
- Dhiraj Joshi, Ritendra Datta, Elena Fedorovskaya, Quang-Tuan Luong, James Z Wang, Jia Li, and Jiebo Luo. 2011. Aesthetics and emotions in images. *Signal Processing Magazine* (2011).
- Tero Karras, Samuli Laine, Miika Aittala, Janne Hellsten, Jaakko Lehtinen, and Timo Aila. 2020. Analyzing and Improving the Image Quality of StyleGAN. In *CVPR*.
- Bingxin Ke, Anton Obukhov, Shengyu Huang, Nando Metzger, Rodrigo Caye Daut, and Konrad Schindler. 2024. Repurposing Diffusion-Based Image Generators for Monocular Depth Estimation. In *CVPR*.
- Eric Kee, James F O'Brien, and Hany Farid. 2013. Exposing photo manipulation with inconsistent shadows. *ACM TOG* (2013).
- Erum Arif Khan, Erik Reinhard, Roland W Fleming, and Heinrich H Bülthoff. 2006. Image-based material editing. *ACM TOG* (2006).
- Diederik P Kingma. 2015. Adam: A method for stochastic optimization. In *ICLR*.
- Alexander Kirillov, Eric Mintun, Nikhila Ravi, Hanzi Mao, Chloe Rolland, Laura Gustafson, Tete Xiao, Spencer Whitehead, Alexander C Berg, Wan-Yen Lo, et al. 2023. Segment anything. In *ICCV*.
- Peter Kocsis, Julien Philip, Kalyan Sunkavalli, Matthias Nießner, and Yannick Hold-Geoffroy. 2024. Lightit: Illumination modeling and control for diffusion models. In *CVPR*.
- Xian Liu, Jian Ren, Aliaksandr Siarohin, Ivan Skorokhodov, Yanyu Li, Dahua Lin, Xihui Liu, Ziwei Liu, and Sergey Tulyakov. 2024. HyperHuman: Hyper-Realistic Human Generation with Latent Structural Diffusion. In *ICLR*.
- Ivan Lopes, Fabio Pizzati, and Raoul de Charette. 2024. Material Palette: Extraction of Materials from a Single Image. In *CVPR*.
- Ilya Loshchilov, Frank Hutter, et al. 2019. Fixing weight decay regularization in adam. In *ICLR*.
- Andreas Lugmayr, Martin Danelljan, Andres Romero, Fisher Yu, Radu Timofte, and Luc Van Gool. 2022. RePaint: Inpainting using Denoising Diffusion Probabilistic Models. In *CVPR*.
- Xiaohe Ma, Valentin Deschaintre, Miloš Hašan, Fujun Luan, Kun Zhou, Hongzhi Wu, and Yiwei Hu. 2024. MaterialPicker: Multi-Modal Material Generation with Diffusion Transformers. arXiv:2412.03225
- Chenlin Meng, Yutong He, Yang Song, Jiaming Song, Jiajun Wu, Jun-Yan Zhu, and Stefano Ermon. 2022. SDEdit: Guided Image Synthesis and Editing with Stochastic Differential Equations. In *ICLR*.
- Rohit Pandey, Sergio Orts-Escolano, Chloe Legendre, Christian Haene, Sofien Bouaziz, Christoph Rhemann, Paul E Debevec, and Sean Ryan Fanello. 2021. Total relighting: learning to relight portraits for background replacement. *ACM Trans. Graph.* (2021).
- Gaurav Parmar, Krishna Kumar Singh, Richard Zhang, Yijun Li, Jingwan Lu, and Jun-Yan Zhu. 2023. Zero-shot image-to-image translation. In *SIGGRAPH*.
- William Peebles and Saining Xie. 2023. Scalable diffusion models with transformers. In *ICCV*.
- Dustin Podell, Zion English, Kyle Lacey, Andreas Blattmann, Tim Dockhorn, Jonas Müller, Joe Penna, and Robin Rombach. 2024. Sdxl: Improving latent diffusion models for high-resolution image synthesis. In *ICLR*.
- Yohan Poirier-Ginter, Alban Gauthier, Julien Phillip, J-F Lalonde, and George Drettakis. 2024. A Diffusion Approach to Radiance Field Relighting using Multi-Illumination Synthesis. In *Computer Graphics Forum*.
- Puntawat Ponglertnapakorn, Nontawat Tritrong, and Supasorn Suwajanakorn. 2023. DiFaReli: Diffusion face relighting. In *ICCV*.
- Alec Radford, Jong Wook Kim, Chris Hallacy, Aditya Ramesh, Gabriel Goh, Sandhini Agarwal, Girish Sastry, Amanda Askell, Pamela Mishkin, Jack Clark, et al. 2021. Learning transferable visual models from natural language supervision. In *ICML*.
- Aditya Ramesh, Prafulla Dhariwal, Alex Nichol, Casey Chu, and Mark Chen. 2022. Hierarchical text-conditional image generation with clip latents. arXiv:2204.06125
- Robin Rombach, Andreas Blattmann, Dominik Lorenz, Patrick Esser, and Björn Ommer. 2022. High-Resolution Image Synthesis with Latent Diffusion Models. In *CVPR*.
- Christoph Schuhmann, Romain Beaumont, Richard Vencu, Cade W Gordon, Ross Wightman, Mehdi Cherti, Theo Coombes, Aarush Katta, Clayton Mullis, Mitchell Wortsman, Patrick Schramowski, Srivatsa R Kundurthy, Katherine Crowson, Ludwig Schmidt, Robert Kaczmarczyk, and Jenia Jitsev. 2022. LAION-5B: An open large-scale dataset for training next generation image-text models. In *NeurIPS*.
- Prafull Sharma, Varun Jampani, Yuanzhen Li, Xuhui Jia, Dmitry Lagun, Fredo Durand, Bill Freeman, and Mark Matthews. 2024. Alchemist: Parametric control of material properties with diffusion models. In *CVPR*.
- Prafull Sharma, Julien Philip, Michaël Gharbi, Bill Freeman, Fredo Durand, and Valentin Deschaintre. 2023. Materialistic: Selecting similar materials in images. *ACM TOG* (2023).
- Jascha Sohl-Dickstein, Eric Weiss, Niru Maheswaranathan, and Surya Ganguli. 2015. Deep unsupervised learning using nonequilibrium thermodynamics. In *ICML*.
- Giuseppe Vecchio and Valentin Deschaintre. 2024. MatSynth: A Modern PBR Materials Dataset. In *CVPR*.
- Giuseppe Vecchio, Rosalie Martin, Arthur Roullier, Adrien Kaiser, Romain Rouffet, Valentin Deschaintre, and Tamy Boubekeur. 2024. Controlmat: a controlled generative approach to material capture. *ACM TOG* (2024).
- K. Yan, F. Luan, M. Hašan, T. Groueix, V. Deschaintre, and S. Zhao. 2023. PSDR-Room: Single Photo to Scene using Differentiable Rendering. In *SIGGRAPH Asia*.
- Hu Ye, Jun Zhang, Sibio Liu, Xiao Han, and Wei Yang. 2023. IP-Adapter: Text Compatible Image Prompt Adapter for Text-to-Image Diffusion Models. arXiv:2308.06721
- Ye Yu, Abhimitra Meka, Mohamed Elgharib, Hans-Peter Seidel, Christian Theobalt, and William AP Smith. 2020. Self-supervised outdoor scene relighting. In *ECCV*.
- Zheng Zeng, Valentin Deschaintre, Iliyan Georgiev, Yannick Hold-Geoffroy, Yiwei Hu, Fujun Luan, Ling-Qi Yan, and Miloš Hašan. 2024. RGBX: Image decomposition and synthesis using material- and lighting-aware diffusion models. In *SIGGRAPH*.
- Lvmin Zhang, Anyi Rao, and Maneesh Agrawala. 2023. Adding Conditional Control to Text-to-Image Diffusion Models. In *ICCV*.
- Qinsheng Zhang and Yongxin Chen. 2021. Diffusion normalizing flow. *NeurIPS* (2021).
- Zitian Zhang, Frédéric Fortier-Chouinard, Mathieu Garon, Anand Bhattad, and Jean-François Lalonde. 2025. Zerocomp: Zero-shot object compositing from image intrinsics via diffusion. In *WACV*.